

A review of polymer multijunction solar cells

Mahbube Khoda Siddiki, Jing Li, David Galipeau and Qiquan Qiao*

Received 11th December 2009, Accepted 26th March 2010

First published as an Advance Article on the web 4th June 2010

DOI: 10.1039/b926255p

Polymer solar cells are one of the most promising prospects for widespread renewable energy due to their low cost, light weight, and mechanical flexibility. However, to date, low efficiencies (7.9%) of these devices inhibit their application. New materials and device designs are needed to increase the efficiency and make this technology available for large-scale applications. A polymer multijunction solar cell made of two or more subcells in series, parallel, or other special connections offers a potential solution to the losses in the current polymer single-junction solar cells. In this article, the recent developments in polymer multijunction photovoltaic materials, cell structures, and device modelling are reviewed. In addition, the current challenges that need to be addressed to achieve significantly higher efficiency are discussed.

1. Introduction

There is increasing global interest in alternative forms of energy, and sunlight is a particularly promising clean and readily available source compared with conventional fossil fuels. Solar cells are devices that directly convert solar energy into electricity. The energy from the sun that strikes the earth is a gigantic 3×10^{24} J a year, or about 10 000 times more than what the global population currently consumes. Covering 0.1% of the Earth's surface with solar cells at an efficiency of 10% would provide the current energy needs of the whole world.¹ However, the electricity generated from solar cells today is less than 0.1% of the world's total energy demand.²

Existing silicon solar cells typically require sophisticated high temperature processing, high quality silicon, and complex engineering, and are therefore not cost effective as an energy source for most applications.³ In addition, these cells have very limited mechanical flexibility. Polymer solar cells show great potential as a low cost alternative to Si solar cells because they can be fabricated using inexpensive painting or simple printing.^{4,5} The advantages of polymer cells include low cost, lightweight and mechanical flexibility.⁶

Polymer solar cells have received increasing interest since 1992 when Sariciftci *et al.*⁷ observed efficient photoinduced electron transfer from polymer semiconductors (conjugated polymers) to an electron acceptor, C₆₀. A power conversion efficiency of 6–7.9% was within reach using conducting polymers as electron donor materials (Fig. 1).^{8–11} Conjugated polymers offer an attractive approach for increasing solar cell efficiencies because their bandgaps and energy levels can be engineered by modifying their chemical structure.

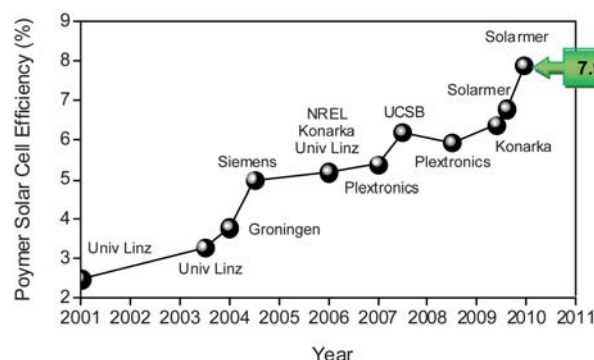


Fig. 1 Efficiency evolution of state of the art polymer solar cells from 2001 to 2009. Some of the efficiency data were taken from ref. 8, 11, 12 and 13.

Center for Advanced Photovoltaics, South Dakota State University, Brookings, SD, 57007, USA. E-mail: Qiquan.Qiao@sdstate.edu.; Fax: +1 605 688 4401; Tel: +1 605 688 6965

Broader context

There is increasing global interest in alternative forms of energy, and sunlight is a particularly promising clean and readily available source compared with conventional fossil fuels. Existing silicon solar cells typically require sophisticated high temperature processing, high quality silicon, and complex engineering, and are therefore not cost effective as an energy source for most applications. Polymer solar cells show great potential as a low cost alternative to Si solar cells because they can be fabricated using inexpensive painting or simple printing. However, to date, low efficiencies of these devices inhibit their application. New materials and device designs are needed to increase the efficiency and make this technology available for large-scale applications. A multijunction polymer solar cell made of two or more subcells in series, parallel, or other special connections offers a potential solution to the losses in the current single junction polymer solar cells to achieve significantly higher efficiency.

However, due to the low carrier mobilities and short carrier diffusion lengths in existing conjugated polymers, the active layer thickness cannot be arbitrarily increased to allow for full spectrum photon flux absorption in a single-junction solar cell. One promising way to achieve this is to use variable bandgap polymers in a tandem structure in which multiple subcells with different energy gaps are stacked.^{14–19} In a multijunction cell, where the subcells are electrically connected in series, the overall open circuit voltage (V_{oc}) is the sum of those from all individual subcells, while the current is the same as that in a single subcell once their currents are matched.²⁰ Other approaches for polymer multijunction solar cells, including parallel connections, mechanical stacking, folded reflective orientation, and

self-passivating structures, have also been studied to increase cell efficiency and performance.^{21–24}

In this paper, the recent developments of polymer multijunction solar cells are reviewed. First, the mechanism, theory, and cell modelling of polymer based single and multijunction solar cells are introduced. Second, the donor polymers, acceptors, and interfacial layer materials are described. Third, polymer multijunction solar cell architectures are discussed in detail for four structures: series connection, parallel connection, mechanical stacking, and folded-reflective orientation. Various processing methods of the interfacial layers including sputter coating, solution processing, thermal evaporation, and the combined solution processing and thermal evaporation are also



Mahbube Khoda Siddiki

Mahbube K. Siddiki received his MS on Materials for Energy Storage and Conversion (MESC) and ME in Energy Technology. He carried out his master research project on Dye Sensitized Solar Cells (DSSCs) under the supervision of Dr Monica Lira-Cantu at Nanoscience and Nanotechnology Research Center (CIN2), Barcelona, Spain. Upon graduation, he joined the Organic Electronics Laboratory of South Dakota State University in 2008. Currently he is

pursuing his PhD under the direction of Dr Qiquan Qiao in the area of Organic Multijunction Solar Cells.



David Galipeau

David W. Galipeau received a BS degree in Electrical Engineering from the University of Rhode Island in 1971 and MS and PhD degrees in Electrical Engineering from the University of Maine in 1989 and 1992. He then joined the faculty at South Dakota State University where he is a Professor of Electrical Engineering, Graduate Coordinator and the Coordinator of the SDSU Photovoltaics Research Group. His research interests include photovoltaic devices, nanotechnology and sensors. He

has received several awards as Distinguished Researcher and Entrepreneur at South Dakota State University. Three of his technical papers have also won awards.



Jing Li

Jing Li received his PhD degree at the Institute of Chemistry, Chinese Academy of Sciences (ICCAS) under the supervision of Prof. Zhishan Bo on the synthesis and characterization of Organic Light-Emitting Diode (OLED) materials in 2006. He then joined Dr Kevin Cheuk's team in working on functional polymers at the Hong Kong Polytechnic University, China. At the end of 2008, he joined Dr Qiquan Qiao's group

to work on low bandgap polymers for photovoltaics at the South Dakota State University, USA.



Qiquan Qiao

Qiquan Qiao obtained his MS degree in Optics from the Shanghai Institute of Optics and Fine Mechanics, Chinese Academy of Sciences, and PhD degree in Engineering from the Virginia Commonwealth University. In 2006 he joined Prof. John Reynolds at the University of Florida as a Post-doctoral Researcher. In 2007 he joined the faculty at South Dakota State University where he established the Organic Electronics Laboratory. Current research includes organic

photovoltaic materials and devices. He received the 2009 Bergmann Memorial Research Award from the US–Israel Binational Science Foundation and 2010 Early Career Award from the National Science Foundation.

described. Finally, current challenges in increasing the efficiencies of polymer multijunction solar cells are presented.

2. Mechanism and theory

2.1 Mechanism and theory of polymer single-junction solar cells

In a polymer single-junction solar cell, illustrated in Fig. 2, the conversion of a photon into an electron–hole pair is able to do the work of qV_{oc} (q : electron charge and V_{oc} : open circuit voltage). This process typically takes six steps as follows, where η is the efficiency of each step:

- 1) Photon absorption (η_A);
- 2) Exciton generation (η_{ex});
- 3) Exciton diffusion (η_{diff});
- 4) Exciton dissociation (η_{ed});
- 5) Charge transport (η_{tr});
- 6) Charge collection (η_{cc}).

Absorbed photons generate excitons (electron–hole pairs), instead of free carriers in the active materials of the polymer solar cells. The excitons must diffuse to the donor–acceptor interface, where they dissociate into free carriers (electrons and holes). These free carriers then transport to their corresponding electrode through a bi-continuous interpenetrating pathway, and are finally collected at the electrodes. Associated with these steps in a single junction solar cell are limitations and losses that include:

- (i) Absorption loss—Spectral mismatch leading to incomplete absorption of low energy photons;
- (ii) Thermalization loss—Conversion of photon energy into a lower energy;
- (iii) Exciton loss;
- (iv) Energy loss required for exciton dissociation;
- (v) Charge recombination.

The above limitations and losses reduce the energy conversion efficiency of a polymer single-junction solar cell. Fig. 3 is a Scharber contour plot which shows the dependence of calculated energy conversion efficiencies *versus* the bandgaps and the LUMO energy levels of light absorbing polymers.²⁵ The highest theoretical energy conversion efficiency for a single-junction

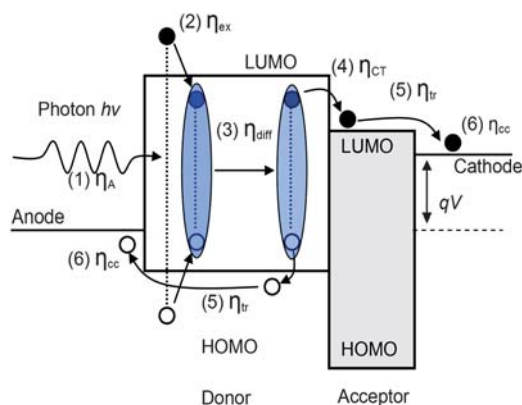


Fig. 2 Energy level diagram of a donor–acceptor (D–A) polymer photovoltaic cell showing six steps associated in device operation. LUMO: lowest unoccupied molecular orbitals; HOMO: highest occupied molecular orbitals; and $h\nu$: photon energy.

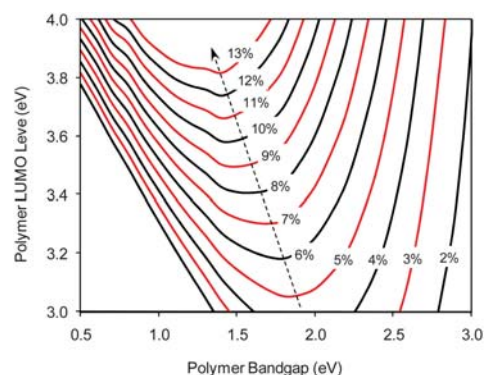


Fig. 3 A Scharber contour plot showing the dependence of calculated energy conversion efficiencies *versus* the bandgaps and LUMO energy levels of the light absorbing (donor) polymers. In this calculation, we assumed: Fill factor (FF) = 0.65 and incident photon to current efficiency (IPCE) = 60%.²⁵

polymer solar cell is about 10–13% for a polymer with a bandgap of 1.5 eV. However, further increase in the efficiency using single junction approaches will be very challenging. Fortunately, multijunction structures have appeared as a promising solution to achieve a higher efficiency in polymer solar cells.

2.2 Mechanism and theory of polymer multijunction solar cells

A polymer multijunction solar cell (PMSC) structure can reduce the previously mentioned losses (i), (ii) and (iv). Absorption loss (i) can also be reduced by employing a multijunction solar cell with a series connection between adjacent subcells, in which the semiconducting polymers with different bandgaps are stacked to absorb a broader spectrum of photons within the solar spectrum.^{14–19} Due to low carrier mobilities and short diffusion lengths, the active layer thickness in single junction cells cannot be arbitrarily increased for efficient broader spectrum absorption. Thus a multijunction structure must be realized using interfacial middle electrodes to collect the carriers from corresponding subcells.

Thermalization loss (ii) can also be reduced by using a multijunction structure made of multiple polymers with different bandgaps. In this way low energy photons are converted to low energy excitons in a low bandgap polymer. Similarly medium and high energy photons are converted into medium and high energy excitons in a medium and high bandgap polymer, respectively.

In addition, a multijunction structure can also help to overcome the energy loss required for exciton dissociation (iv). In order for charge transfer to occur efficiently, the offset between the donor LUMO and acceptor LUMO needs to be high enough to overcome the exciton binding energy, which is typically 0.1–0.4 eV. In a P3HT:PCBM system, the offset is large at almost 1.4 eV which sacrifices V_{oc} . Fig. 4 shows cell efficiency *versus* bandgap for various donor–acceptor LUMO offsets and indicates that polymer single-junction solar cell efficiency can be increased from about 5% to above 15% when the energy loss required for exciton dissociation (offset) is reduced from 1.0 eV to 0.2 eV. In a polymer solar cell V_{oc} can be estimated from the difference between the donor HOMO and acceptor LUMO.

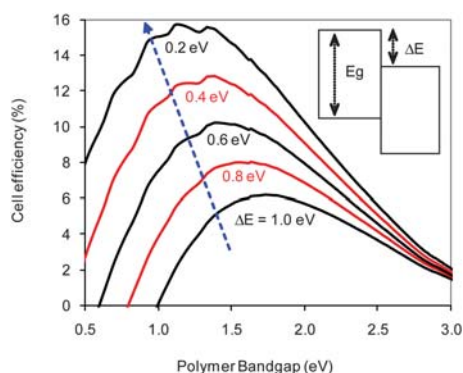


Fig. 4 Dependence of energy conversion efficiency (η) on the bandgap (E_g) of donor polymers and the offset (ΔE) between donor LUMO and acceptor LUMO levels. In our modeling, we assumed: fill factor (FF) = 0.65; incident photon to current efficiency (IPCE) = 60%. These assumptions are realistic since the state-of-the-art polymer solar cells have been capable of achieving FF > 0.6 and IPCE > 70%.^{8,26}

The multijunction structure provides the opportunity to engineer the corresponding offsets in individual subcells for photons from different regions in the solar spectrum. Moreover, in a polymer multijunction solar cell, multiple donor–acceptor systems can be designed for different subcells that harvest photons from various solar spectral regions; however the same donor–acceptor system is used for all the photons in a single junction device.

2.3 Modelling of polymer multijunction cells

Polymer multijunction solar cells consisting of two or more subcells can be modeled as follows.

The short circuit current density of the first subcell (optical front cell), J_{sc1} in a multijunction device under AM1.5G is given by^{27,28}

$$J_{sc1} = \int_{\lambda_0}^{\lambda_1} e \cdot N_{ph}(\lambda) \cdot EQE_1(\lambda) \cdot (1 - M) d\lambda \quad (1)$$

Here, $EQE_1(\lambda)$ and $N_{ph}(\lambda)$ are the external quantum efficiency and photon flux density, respectively, at a wavelength λ in the incident solar (AM1.5G) spectrum. λ_1 is the cutoff absorption wavelength of the first subcell (optical front cell). In a single junction cell, the top electrode (e.g. Al) typically acts a mirror and reflects the transmitted light back to the active layers for additional light absorption. However, in a multijunction solar cell, the interfacial layers (e.g. TiO_2 , ZnO , etc.) do not function as a mirror to reflect the transmitted light. Therefore, compared to single junction cells, the optical front cell has some loss, which is called mirror loss and is represented by M .²⁸ This loss is caused by the absence of significant reflection at the interface between adjacent subcells. It is thickness-dependant and has recently been estimated at ~15% in average, according to transfer matrix based optical simulations.^{27,28}

In contrast to single junction cells, to calculate the short circuit current density (J_{sc2}) of the second subcell (optical back cell) in a multijunction structure, both external quantum efficiency (EQE_1) and internal quantum efficiency (IQE_1) of the optical front subcell are required. λ_2 is the cutoff absorption wavelength

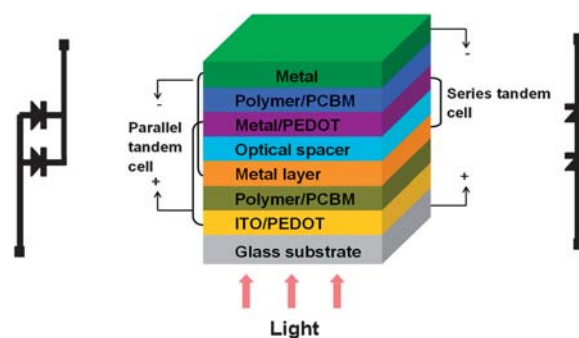


Fig. 5 Schematic diagram of PMSCs in electrically series and parallel connections.

of the second subcell. The short circuit current density of the second subcell (J_{sc2}) in a multijunction device under AM1.5G can be calculated as^{27,28}

$$J_{sc2} = \int_{\lambda_0}^{\lambda_2} e \cdot N_{ph}(\lambda) \cdot EQE_2(\lambda) \cdot \left[1 - \frac{EQE_1(\lambda)}{IQE_1(\lambda)} \cdot (1 - M) \right] d\lambda \quad (2)$$

According to fabrication procedures, a typical multijunction solar cell can be connected in two ways: (i) series; and (ii) parallel. Fig. 5 shows the two basic electrical connections in a multijunction solar cell.

2.3.1 Subcells connected in series. In series multijunction cells, excitons are formed in all subcells during light absorption. After the excitons dissociate at the donor–acceptor (D/A) interface, electrons in one subcell and holes in its adjacent subcell diffuse to the middle contact layer to recombine while the remaining free carriers are collected at the outer electrodes (Fig. 6).²⁹

The overall current is determined by the lowest current produced by the individual subcells in the stack. The current of each subcell can be optimized to be equal to the others at the operating illumination intensity.^{14,30} Otherwise, the extra charges will build some local potential and electric field, and thus reduce device efficiency. The individual subcell currents are typically optimized by varying the thicknesses or material composition of the active materials in each subcell. In addition, optical interference effects and thickness-dependent optical properties of the

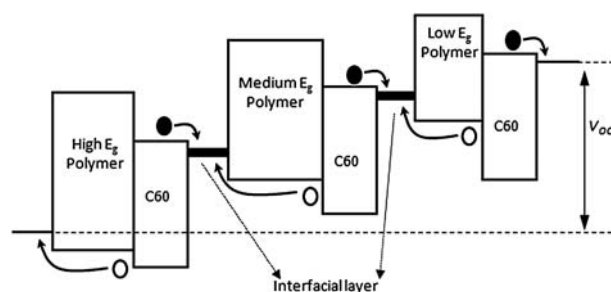


Fig. 6 Energy level diagram of a triple-junction polymer solar cell in a series connection under the open circuit voltage condition showing how the electrons in one subcell and holes in its adjacent subcell will diffuse to the middle contact (interfacial) layer to recombine.^{29,30}

interfacial layers are also important factors and need to be considered.³⁰

An alternative model has been proposed by Hadipour *et al.*³¹ They reported that $J_{\text{sc-multi}}$ of a multijunction device may entirely depend on the combination of short circuit current density (J_{scn}) and fill factor (FF_n) of the individual subcells. For example, a combination of one subcell with a extremely low FF and J_{sc} , and the other one with a much higher FF and J_{sc} may lead to a multijunction cell with a fairly low FF and a high J_{sc} . Then the J_{sc} of the multijunction cell might be equal to the highest J_{sc} in the subcells.

The open circuit voltage (V_{oc}) of a multijunction solar cell in a series connection is the sum of V_{oc} s of the individual subcells, thus it can be written as:

$$V_{\text{oc-multi}} = V_{\text{oc1}} + V_{\text{oc2}} + V_{\text{oc3}} + \dots \quad (3)$$

where V_{oc1} , V_{oc2} , V_{oc3} , ... are the open circuit voltage of the individual subcells in the stack. Typically, the deposition of multiple cells in series results in an inversely-oriented heterojunction between the donor (D) layer of one cell and the acceptor (A) layer of its adjacent cell. The carriers will pile up in the reverse D-A junction and reduce the $V_{\text{oc-multi}}$.³⁰ In order to prevent the carrier build-up, interfacial layers are required to be inserted between the adjacent individual subcells, providing recombination centers for electrons and holes approaching from the adjacent cells and ensuring a maximized $V_{\text{oc-multi}}$.

It is generally agreed that the V_{oc} of subcell i can be estimated from the difference of the acceptor LUMO and donor HOMO as:

$$V_{\text{oc}(i)} = \frac{1}{e} (\text{LUMO}_{\text{acceptor}(i)} - \text{HOMO}_{\text{donor}(i)}) \quad (4)$$

However, this equation needs to be modified in some cases. For example, Scharber *et al.*²⁵ have observed that the open circuit voltage of a polymer/PCBM solar cell could be approximated as:

$$V_{\text{oc}} = \frac{1}{e} (\text{LUMO}_{\text{PCBM}} - \text{HOMO}_{\text{polymer}} - 0.3 \text{ eV}) \quad (5)$$

Where the value of 0.3 eV is an empirical factor which describes the deviation between the theoretical maximum built-in potential (V_{bi}) and the open circuit voltage (V_{oc}). The current understanding of polymer solar cells suggests that the open circuit voltage in individual subcells can be improved either by moving the LUMO of an acceptor closer to the vacuum level (but still having an offset with the donor's LUMO for efficient charge transfer) or pushing the HOMO of a donor away from the vacuum level.^{8,26} Multijunction cell efficiency in a series connection can be calculated as:

$$\eta_{\text{multi}} = \frac{J_{\text{sc-multi}} \cdot V_{\text{oc-multi}} \cdot \text{FF}}{P_{\text{light}}} \quad (6)$$

where the FF can be improved by optimizing film morphology and interfacial layers not only between adjacent individual subcells but also between the active layer and the top or bottom electrode.^{26,32,33}

Fig. 7 shows the theoretical performance of multijunction solar cells connected in series in terms of cell efficiency (η_{multi}), open circuit voltage ($V_{\text{oc-multi}}$), and short circuit current density

($J_{\text{sc-multi}}$), as well as the absorption spectrum region of the optical back cell. The analysis was performed under four assumptions: (1) the individual subcells were connected in series; (2) the acceptor was not a specific material, such as widely used fullerene derivatives, but assumed to have all available LUMO energy levels; (3) each subcell optimally absorbed the same amount of photon flux and generated identical current density, leading to minimal current loss; (4) both the top and bottom electrode had an Ohmic contact with photoactive layers and the contact loss was not considered. The bandgap (E_g) of the donor in individual subcells was obtained from their cutoff absorption wavelengths and the V_{oc} of the individual subcells was estimated by subtracting E_g from the exciton binding energy (E_b). It was also assumed that the FF and IPCE were 0.65 and 60%, respectively. The cell efficiencies of the multijunction solar cells were finally calculated using eqn (6).

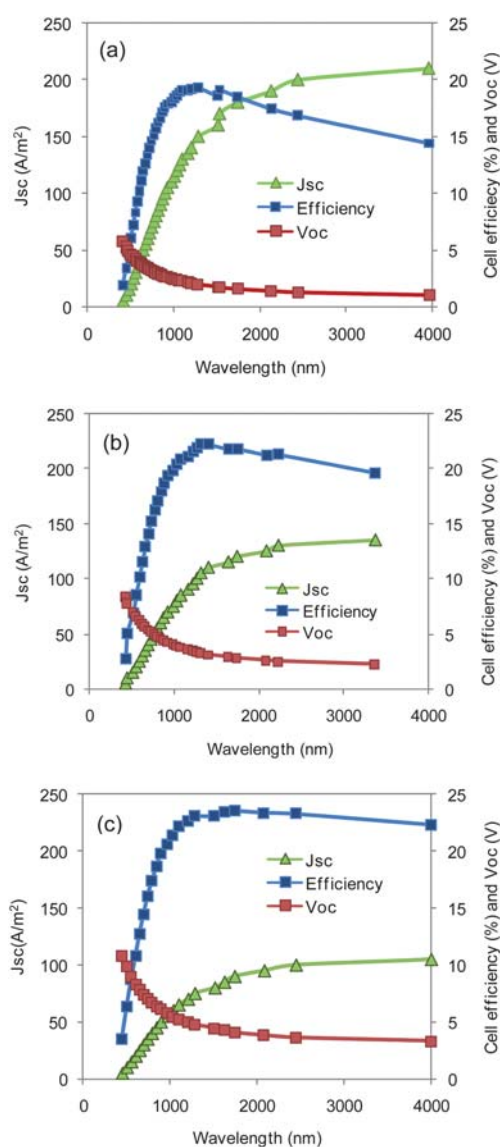


Fig. 7 The theoretical dependence of cell efficiency (η_{multi}), open circuit voltage ($V_{\text{oc-multi}}$), and short circuit current density ($J_{\text{sc-multi}}$) on the absorption spectrum of the optical back cell of: (a) double-junction cells; (b) triple-junction cells; and (c) quadruple-junction cells.

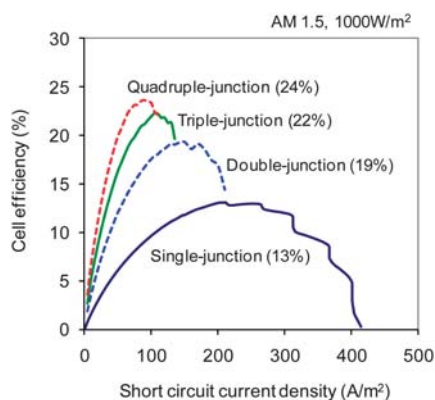


Fig. 8 The effect of the number of subcells and J_{sc} on multi-junction cell efficiency. In our modeling, we assumed: fill factor (FF) = 0.65; incident photon to current efficiency (IPCE) = 60%.

It was found that in a specific multijunction (double, triple, quadruple, ...) case, V_{oc} decreased and J_{sc} increased as the optical back cell's light absorption spectra were broadened to near infrared or infrared regions. It is not always true that multijunction solar cell efficiency increases as the light absorption spectrum is broadened, since the light absorption will only increase the short circuit current density. A balance between the short circuit current density and open circuit voltage needs to be achieved. Once a polymer multijunction solar cell with a fixed number of subcells is designed, an optimal light absorption spectrum range needs to be identified to achieve the highest possible energy conversion efficiency. With a reasonable assumption of FF = 0.65 and IPCE = 60%, the highest achievable energy conversion efficiency in a double, triple, quadruple cell is expected to increase and the maximum efficiency can be obtained when the cutoff light absorption wavelength in the optical back subcell is at about 1150 nm, 1400 nm, and 1740 nm, respectively.

Fig. 8 shows the theoretical dependence of multijunction cell efficiencies on the number of subcells and J_{sc} in the stack with a series connection. The results show that the achievable energy conversion efficiency for a single, double, triple and quadruple-junction polymer solar cell is 13%, 19%, 22%, and 24%, respectively. This demonstrates that multijunction solar cells can substantially increase energy conversion efficiency compared to a single junction solar cell by overcoming the losses mentioned earlier.

3.2.2 Subcells connected in parallel. When the subcells in a PMSC are connected in parallel, the short circuit current density of the device is the sum of J_{sc} s of all individual subcells, thus it can be expressed as:

$$J_{sc\text{-multi}} = J_{sc1} + J_{sc2} + J_{sc3} + \dots \quad (7)$$

And the open circuit voltage of multijunction device ($V_{oc\text{-multi}}$) is the minimum V_{oc} of individual subcells.

3. Polymer multijunction solar cell materials

3.1 Donor polymer materials

Conjugated polymers, as donor materials, are semiconducting due to their framework of alternating single and double

carbon-carbon bonds. Most conjugated polymers have a bandgap between the HOMO and the LUMO in the range of 1.5–3 eV and a high absorption coefficient of $\sim 10^5 \text{ cm}^{-1}$. This makes them well suited for absorbing visible light in photovoltaic devices. However, the optical absorption range is relatively narrow in the solar spectrum because most conjugated polymers only absorb light in the blue and green while absorption in the red and near infrared is quite poor. Narrow band light absorption of the solar spectrum limits photocurrent generation. In addition, donor polymers should have high hole mobility for efficient charge transport. The selection and manipulation of polymer combinations in multijunction cells is very important for achieving a high power conversion efficiency.³⁴ Therefore, in order to increase the cell efficiencies, it is necessary to fabricate multijunction cells with absorption at different spectral responses including the near infrared and infrared regions, and to stack them together.³⁵

To efficiently harvest broad spectrum sunlight, low bandgap polymers ($E_g < 1.8 \text{ eV}$) are needed to improve light harvesting.^{44–46} Recently, these polymers have been successfully applied in polymer multijunction solar cells as an optical back subcell in combination with high bandgap polymers as optical front subcells.^{40,47,48} Table 1 lists the common conjugated polymers as donors including the most recently developed low bandgap polymers. Fullerene derivatives (*e.g.* PCBM and PC₇₀BM) were used as the acceptors listed in Table 1 to compare efficiencies.

3.2 Acceptor materials

The acceptor materials in polymer solar cells need to have a higher electron affinity than the donor polymers. In other words, the LUMOs and HOMOs of the acceptor materials need to lie well below the related LUMOs and HOMOs of various donor polymers, making them energetically favorable for exciton dissociation and charge transfer at the interfaces. A high electron accepting ability is also required for applications in solar cells. For example, buckminsterfullerene is capable of taking up to six electrons.⁵⁴ Another property is their high electron mobility, which works as a “speed limit” for electron transport. Table 2 lists typical fullerene-based acceptor materials.^{9,49}

3.3 Interfacial layer materials

Transition metal oxides (*e.g.* TiO_{x(x≤2)} and ZnO), transparent conductive oxides such as indium tin oxide, and metallic nano-clusters (*e.g.* Au and Ag nano-clusters) are often used as interfacial or recombination layers in PMSCs (Table 3).^{9,19,50,55} These layers act as a protecting layer for the bottom subcell and a base for the top cell. The transparency of the interfacial layers should be considered along with their electrical properties, since light blocking from the interfacial layers can reduce the light that will be absorbed by the back subcells. Transparent metal oxides such as TiO_{x(x≤2)} and ZnO serve as an electron transport and collecting layer for the first subcell and as a stable base for the second subcell fabricated on its top.⁹ Conducting polymers (*e.g.* PEDOT:PSS and modified PEDOT) and other transitional metal oxides (*e.g.* V₂O₅, MoO₃, *etc.*) can act as a hole-transport layer.⁵⁰ With the help of a multilayer semitransparent electron or hole transport interlayer, two or more polymer subcells can be

Table 1 Non-exhaustive list of typical polymer donor materials in PMSCs

Structure	Name	HOMO/eV	LUMO/eV	Bandgap/eV	Cell efficiency (%)		Ref.
					Single-junction	Multi-junction	
	PBDTTT-CF: poly[4,8-bis-substituted-benzo[1,2- <i>b</i> :4,5- <i>b'</i>]dithiophene-2,6-diyl- <i>alt</i> -4-substituted-thieno[3,4- <i>b</i>]thiophene-2,6-diyl]-derived polymer	−5.22	−3.45	1.77	6.77%	—	8
	PCDTBT: poly[<i>N</i> -9'-hepta-decanyl-2,7-carbazole- <i>alt</i> -5,5-(4',7'-di-2-thienyl-2',1',3'-benzothiadiazole)]	−5.5	−3.6	1.9	6.1%	—	26
	PBTTQ: alternating electron-rich bithiophene and electron-deficient thiadiazoloquinoxaline units	−4.7	−3.75	0.94	0.08%	—	36
	PDDTT: poly(5,7-bis(4-decanyl-2-thienyl)thieno[3,4- <i>b</i>]diathiazole thiophene-2,5)	−4.71	−3.59	1.12	0.11%	—	37
	PTBEHT: poly(5,7-di-2-thienyl-2,3-bis(3,5-di(2-ethylhexyloxy)phenyl)thieno[3,4- <i>b</i>]pyrazine)	—	—	1.2	1.1%	0.57%	29, 38
	PBEHTT: (poly(5,7-bis[3,4-di(2-ethylhexyloxy)-2-thienyl]-2,3-diphenylthieno[3,4- <i>b</i>]pyrazine))	—	—	1.28	0.29%	—	38
	PCPDTBT: poly[2,6-(4,4-bis-(2-ethylhexyl)-4 <i>H</i> -cyclopenta[2,1- <i>b</i> ;3,4- <i>b'</i>]dithiophene- <i>alt</i> -4,7-(2,1,3-benzothiadiazole)]	−4.9	−3.5	1.4	3.2%	6.5%	9, 39
	PTPTB: poly-(<i>N</i> -dodecyl-2,5-bis(2'-thienyl)pyrrole-(2,1,3-benzothiadiazole))	−5.5	−3.73	1.77	1%	—	40
	P3HT: poly(3-henxylthiophene)	−5.2	−3.2	2	4.4%	6.5%	9, 41
	MDMO-PPV: poly[2-methoxy-5-(3',7'-dimethyloctyloxy)-1,4-phenylenevinylene]	−5.0	−2.8	2.2	3.3%	3.1%	17, 42
	PFDTBT: poly((2,7-(9,9-dioctyl)-fluorene)- <i>alt</i> -5,5-(4',7'-di-2-thienyl-2',1',3'-benzothiadiazole))	−5.5	−3.6	1.9	4.5%	0.57%	29, 43

Table 2 Non-exhaustive list of typical acceptor materials.^{9,49}


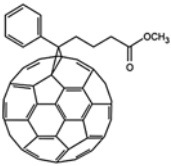
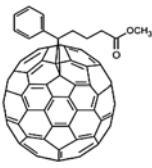
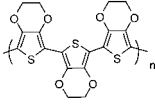
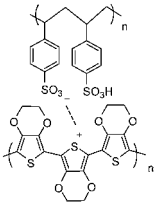
Structure	Name	HOMO/eV	LUMO/eV	Bandgap/eV	Ref.
	C ₆₀	−6.2	−4.5	1.7	49
	[60]PCBM: [6,6]-phenyl C ₆₁ butyric acid methyl ester	−6.1	−4.3	1.8	9
	[70]PCBM: [6,6]-phenyl C ₇₁ butyric acid methyl ester	−6.1	−4.3	1.8	8

Table 3 Non-exhaustive list of materials typically used as interfacial layers in PMSCs (ETL: electron transport layer; HTL: hole transport layer)

Name/structure	HOMO/eV	LUMO/eV	Bandgap/eV	Work-function/role	Ref.
TiO ₂ /TiO _x	−8.1	−4.4	3.7	ETL	9
ZnO	−7.5	−4.2	3.3	ETL	19
MoO ₃	−5.3	−2.3	3.0	HTL	50
V ₂ O ₅	−6.55	−4.25	2.3	HTL	51
ITO	—	—	—	4.8/ETL	17
	—	—	—	5/HTL	19
PEDOT	—	—	—	5.2/HTL	9,52,53
	—	—	—		
PEDOT:PSS					

stacked together. Table 3 shows a non-exhaustive list of materials typically used as interfacial layers in PMSCs.

TiO_x ($x \leq 2$) and ZnO can also be used as an optical spacer, a transparent electron transport layer between the metal top electrode and active layer, to place the active layer into a more favorable region of the internal electrical field. An embedded optical spacer can separate two photoactive single cells and optimize the electronic and optical properties of the whole cells. Polymer solar cells whose film thicknesses are limited by low charge carrier mobility can benefit from an optical spacer layer.^{26,56,57}

4. PMSC device structures

An enormous number of scientific papers dealing with polymer multijunction solar cells have been published in the last several

years. Several approaches including series connections, parallel connections, mechanical stacking, and folded reflective structures in PMSCs have been discussed by various groups. In this section, different structures of polymer multijunction solar cells and their performance are described.

4.1 Series cell structure

4.1.1 Normal structure. In the normal structure, subcells made of polymeric semiconductors with different bandgaps are fabricated into one multijunction cell, in which the wide bandgap polymer is used in the optical front cell (bottom cell) while the narrow bandgap polymer is placed in the optical back cell (top cell). Fig. 9 represents a typical monolithic normal structure of a PMSC consisting of two subcells. The bottom cell with wide

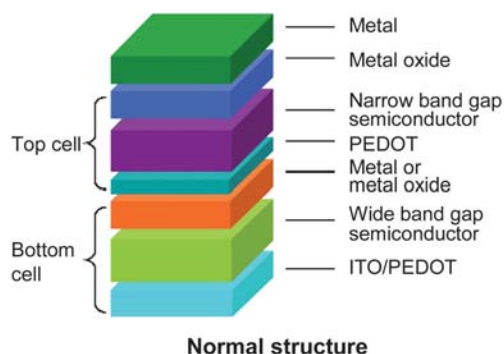


Fig. 9 Schematic diagram of a PMSC with normal series connection structure.

bandgap materials absorb high energy photons and let the low energy photons pass through which are absorbed by the low bandgap material in the top cell.^{14,19,22,23,29,58}

4.1.2 Inverted structure. In an inverted polymer multi-junction solar cell structure, narrow bandgap polymers are used in an optical front subcell (bottom cell) while wide bandgap polymers are in the optical back subcell (top cell). This structure is selected when the narrow bandgap polymer must be made quite thin to get optimum performance while its absorption spectrum does not overlap too much with that of the wide bandgap polymers used in the top subcell. Kim *et al.*⁹ observed that the inverted structure (Fig. 10a) led to the highest efficiency when P3HT and PCPDTBT were used as an active material in the subcells. The absorption spectra of P3HT and PCPDTBT are illustrated in Fig. 10b. The authors studied all possible variations of the multijunction cell architectures to optimize and balance the current in the subcells. They changed the order of the active materials (*i.e.* normal and inverted structures), varied the concentration and ratio of each component in the composite solutions, and optimized the thickness of the active materials in the subcell. It was found that the P3HT:PC₇₀BM back cell had a smaller J_{sc} between the two subcells and thus limited the overall cell performance because the PCPDTBT:PCBM front subcell had a higher extinction coefficient. The authors also observed that the FF of the multijunction cell was very close to, and determined by, that of the limiting subcell. Therefore, they used the P3HT:PC₇₀BM as the back subcell to obtain a higher FF and improved performance.

4.1.3 Self passivating structure. A self passivating multi-junction photovoltaic device, consisting of a PbSe nanocrystal quantum dot photoconductor as the optical front subcell and a P3HT/PCBM as the back subcell, was reported by Kim *et al.*²⁴ As shown in Fig. 11a and b, the PbSe quantum dot front subcell served as both a photocurrent generator and a UV protector for the back cell made of P3HT/PCBM. The authors claimed that this structure had four major advantages: (1) all-solution based processing; (2) provided UV degradation protection for the polymer based back subcell; (3) the protective layer had multiple exciton generation resulting in higher UV energy conversion efficiency; and (4) the polymer back subcell provided an electric field to extract charges generated from the PbSe quantum dot

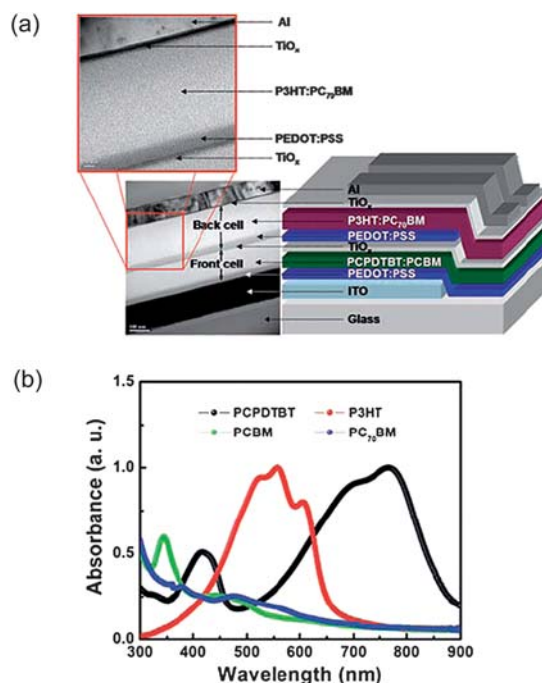


Fig. 10 (a) The device structure (right) and TEM cross-sectional image (left) of the polymer tandem solar cell. (b) Absorption spectra of low bandgap PCPDTBT (optical front subcell), high bandgap P3HT (back subcell) films, and the acceptor materials including PCBM and PC₇₀BM. Reprinted with permission from ref. 9.

layer. This multijunction device had lower overall performance ($\eta = 1.17\%$, $V_{oc} = 0.57$ V, $J_{sc} = 6.38$ mA cm⁻²) than single-junction cells due to inefficient photocurrent extraction from the PbSe layer caused by traps and defects on the nanocrystal surface. However, as shown in Fig. 11c, stability measurements under AM 1.5 and UV-enhanced illumination on both the double-junction device and the reference P3HT/PCBM cell demonstrated that the PbS quantum dot film did improve the robustness of multijunction cells. The double-junction cells also showed significantly higher durability than the control polymer solar cells because of the UV protection from the optical front PbSe subcell.

4.2 Parallel cell structure

Zhang *et al.*²¹ reported a simple structure of a multijunction device that represents an alternative way to connect two subcells in parallel. The schematic diagram of the cell and its equivalent circuit diagram are depicted in Fig. 12. In this device, a PCBM layer was used to form both a bilayer heterojunction subcell with the underlying CuPc layer and a bulk-heterojunction subcell blended with P3HT. The disadvantage of this design was that only excitons created within the exciton diffusion lengths at the CuPc/PCBM interface in the bilayer subcell were able to diffuse to the interface for separation into free carriers.

The enhanced short circuit current density ($J_{sc} = 8.63$ mA cm⁻²) and power conversion efficiency (PCE = 2.79%) of the parallel double-junction solar cells were close to the sum of those from the individual subcells of CuPc/PCBM ($J_{sc} = 2.09$ mA cm⁻² and PCE = 0.43%) and P3HT:PCBM ($J_{sc} = 6.87$ mA cm⁻² and

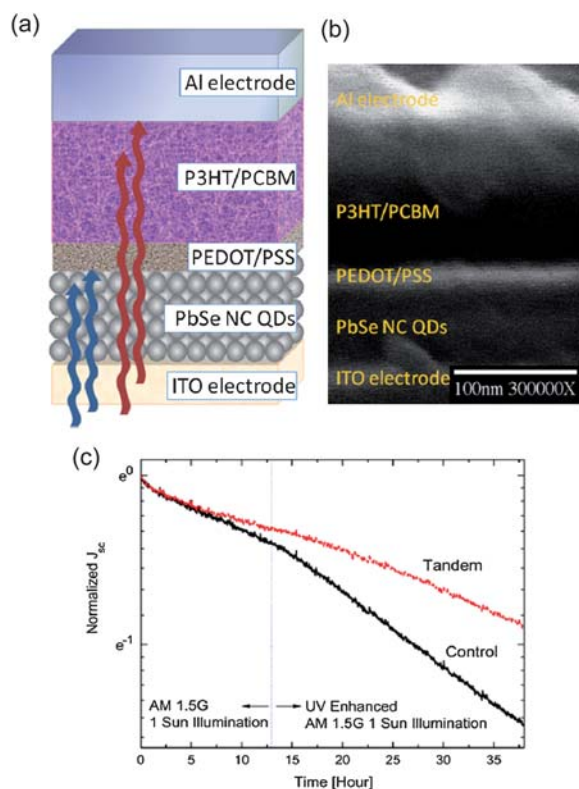


Fig. 11 (a) Self-passivating double junction solar cell structure that includes an additional photoconductive PbSe nanocrystal film layer. (b) Cross-sectional SEM image of the device. The thickness of each layer was 80 nm (P3HT/PCBM), 30 nm (PEDOT) and 50 nm (PbSe), respectively. (c) Stability test results for the double junction and reference P3HT/PCBM cells under AM1.5G illumination and UV-enhanced illumination showing that the self passivating front subcell improved the overall cell durability. Reprinted with permission from ref. 24.

PCE = 2.5%). Compared to the above-described series multi-junction cells, the parallel cell design did not require transparent or semitransparent intermediate layers. Thus the device configuration was simplified for lower cost. In addition, the light absorption loss in the optical back cell was also significantly reduced.

4.3 Mechanically stacked structure

When the active layer of each subcell in a multijunction device is formed by solution processing, PMSC fabrication becomes quite challenging since the formation of the additional middle or back subcells may damage the transparent/semitransparent intercell connection layers and the front subcell that has already been fabricated. Shrotriya *et al.*²² reported an approach to overcome the processing difficulties in solution based multijunction cells. They fabricated two identical bulk heterojunction single cells on different glass substrates and then positioned them on top of each other. Depending on the need, the subcells were connected either in series or in parallel outside the device. Both subcells had identical active materials (MEH-PPV:PCBM blend) about 70 nm thick. The bottom cell had a semitransparent cathode consisting of 1 nm LiF, 2.5 nm Al and 12.5 nm Au, which showed a maximum transparency of ~80% at 580 nm. It was reported

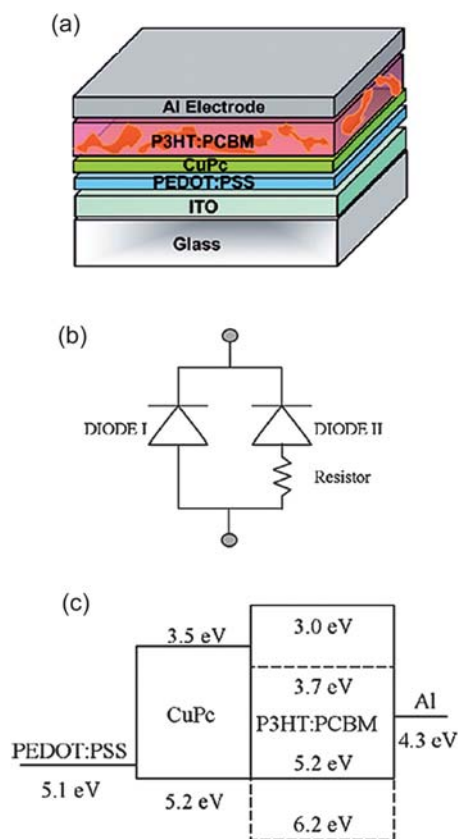


Fig. 12 (a) The cell structure of PMSC connected in parallel; (b) the equivalent circuit diagram; and (c) the energy level diagram. The extra resistor shown in (b) indicated that holes generated in the blend layer had to be transported across the CuPc layer. Reprinted with permission from ref. 21 and 27.

that an increase of the active layer thickness in PPV-based solar cells led to enhanced absorption, but not improved performance.⁵⁹ However, this was solved by using two identical thin active layers in each subcell of the mechanically stacked cell, which effectively increased absorption while maintaining favorable electrical properties. A schematic diagram of the mechanically stacked cell structure and its current density–voltage curves are shown in Fig. 13.

The subcells in both the series and parallel configurations had an active layer thickness of ~70 nm. It was found that the efficiency of ~2.5% for both the parallel and series cells was equal to the efficiency of a single layer device with a thickness of 140 nm. Therefore the coupling of two identical subcells did not have an efficiency advantage *versus* a single cell with the same total active layer thickness. A summary of their results is given in Table 4. The main advantage of this structure is flexibility in cell orientation.

4.4 Folded reflective structure

A new architecture for multijunction solar cells, called “folded reflective multijunction device” was reported by Tvingstedt *et al.*²³ This is another approach to the general challenges of multijunction cells including extra transparent/semitransparent interlayer electrodes and solvent incompatibility. The authors

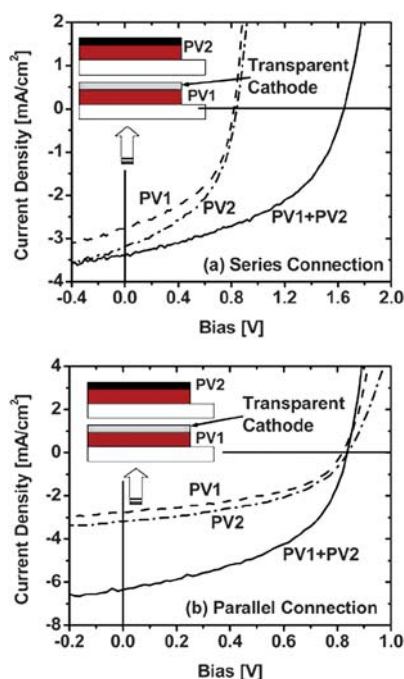


Fig. 13 Current density–voltage curves for the mechanically stacked multiple-cell structure in (a) series connection, and (b) parallel connection. The inset is the device structure. Reprinted with permission from ref. 22.

Table 4 Performance of mechanically stacked solar cells processed on separated substrates.²²

Cells		V_{oc}/V	$J_{sc}/mA\ cm^{-2}$	FF [%]	η [%]
Bottom		0.86	2.6	45	1.1
Top		0.86	3.2	45	1.3
Multijunction	Series	1.64	3.4	45	2.4
	Parallel	0.84	6.3	45	2.5

demonstrated that single subcells reflect nonabsorbed light to adjacent subcells thereby improving efficiency. By folding two substrates with a single subcell built on each top, substantial enhancement in the cell efficiency was obtained due to light trapping. In addition, this structure provided an opportunity to fabricate multijunction solar cells with arbitrary optical and electrical connections in either series or parallel. It was found that the folded multijunction cell efficiency in series connection increased from 2.0% to 3.7% as the fold angle increased from 0° to 70°.

Using a similar design, Zhou *et al.*⁶⁰ demonstrated an array of reflective multijunction cells by folding four individual subcells on a single plastic substrate. Fig. 14 shows the folded cell structure. The authors observed that the increase of cell efficiency was negligible when the opening angle was larger than 120° because the reflected light from one subcell was not directed to the adjacent subcells. However, cell efficiencies were significantly improved by $62\% \pm 12\%$ at an angle of 30° compared to a planar cell in either the series or parallel configurations. With a series connection of four subcells, an open circuit voltage of 3.45–3.65 V was achieved at an opening angle of 30°.

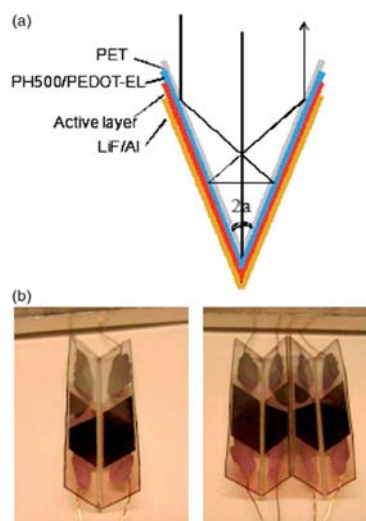


Fig. 14 (a) Device configuration and light ray paths for a folded reflective cell at an opening angle of $2a$. (b) Pictures of the cell arrays consisting of two subcells (V-geometry) and four subcells (W-geometry). Reprinted with permission from ref. 60.

5. Interface engineering

Typically, the active layers of the subcells in PMSCs are fabricated by solution based processes including spin coating, ultrasonic spray coating, and potentially large-scale roll-to-roll processing.^{9,19,53,61,62} However, these techniques have several challenges. The major difficulty lies in the stacking ability, *i.e.* probable dissolution or damage of lower layers during the deposition of top cells, especially when the same or similar solvents are used. Various special techniques including the previously described mechanically stacked multi-cell structure and the folded reflective multijunction cells have been used to address these issues. Recently a new type of multijunction solar cell using thermocleavable polymers has also been reported, in which additional subcell layers are deposited by converting the earlier deposited subcells from a soluble to an insoluble form *via* thermal annealing. However, the cell efficiencies using these new approaches were lower than those of traditional series connection approaches.⁵³ Thus a majority of current research has been focused on the PMSC structure in series. In these cells, a separating layer (middle contact) is required that has to be: (i) thick enough to protect the bottom subcell from dissolving during solution processing of the top subcell; (ii) strong enough to act as foundation for the top subcell; and (iii) transparent or semitransparent for efficient light transfer to the top cell. In addition, the middle electrode interfacial layer should provide an Ohmic contact between the two adjacent subcells. To overcome the fabrication issues of subcell stacking, different processing methods, as well as new materials have been reported and are reviewed in this section.

5.1 Sputter coating

Kawano *et al.* reported a double-junction solar cell comprised of two bulk heterojunction (BHJ) subcells connected in series with a interlayer of indium tin oxide (ITO).¹⁷ Due to high

Table 5 Average open circuit voltage of the subcells and the multijunction cells; Cell A: Glass/ITO/PEDOT:PSS/MDMO-PPV:PCBM/ITO; Cell B: Glass/MDMO-PPV:PCBM/ITO/PEDOT:PSS/MDMO-PPV:PCBM/Al; Double junction: Glass/ITO/PEDOT:PSS/MDMO-PPV:PCBM/ITO/PEDOT:PSS/MDMO-PPV:PCBM/Al. Reprinted with permission from ref. 17

BHJ organic solar cell	Open circuit voltage, V_{oc}/V
Cell A	0.48 ± 0.04
Cell B	0.73 ± 0.01
Stacked	1.31 ± 0.04

transparency of the ITO layer, the light intensity reaching the top cell was very high, resulting in increased photocurrent in the top cell. The ITO separating layer, acting as electron transport layer, could be deposited either by spin-coating, rf or dc magnetron sputtering. PEDOT:PSS was used as the hole transport layer. Table 5 shows the average open circuit voltages (V_{oc}) of the individual subcells and stacked double-junction cells under 100 mW cm^{-2} AM1.5G illumination.

The V_{oc} s of the individual subcells were separately evaluated. The V_{oc} of the stacked cell was found to be the sum of the V_{oc} s of the individual subcells (A and B), indicating that the subcells were connected in series.

5.2 Solution processing

5.2.1 ZnO interlayer. A solution-processed ZnO middle electrode opened the possibility for fully solution-processed multijunction cells.¹⁹ ZnO nanoparticles were prepared,^{63,64} dispersed in acetone, and spin-coated on top of the active layer of the bottom cell as an electron transport layer (ETL). For the hole transporting layer (HTL), neutral pH PEDOT:PSS was spin-coated from a water based suspension. The active layers were fabricated from a chlorobenzene solution of a composite made of donor (MDMO-PPV or P3HT) and acceptor (PCBM).

Due to large energy offset and non-Ohmic contact at the interface between ZnO and neutral pH PEDOT, charge recombination across this interface was poor. This problem was overcome *via* photodoping ZnO by exposure to UV light for a few seconds.^{65,66} This resulted in an Ohmic contact between the ZnO and PEDOT which prevented a voltage drop (or loss) across the interface and allowed the holes and electrons to recombine efficiently. Fig. 15 shows multijunction solar cell performance in terms of V_{oc} , J_{sc} , FF, and P_{max} . With photodoping of ZnO by UV, device efficiency improved by 50% and an V_{oc} of 2.19 V was obtained for a triple-junction cell. This V_{oc} was close to the sum of the individual subcell V_{oc} s.

A ZnO interlayer was also used in all-solution processing for a PMSC based on thermocleavable polymers reported by Hagemann *et al.*⁵³ This gave flexibility in processing layers that could be converted from a soluble to an insoluble form using a short thermal annealing step. Thus the problems associated with solubility during the deposition of subsequent layers were effectively solved. Schematic diagrams of the device structures are shown in Fig. 16.

In this approach, a branched alkyl chain was used as a solubilizing group which was attached to the active conjugated polymer backbone through an ester group. When heated this

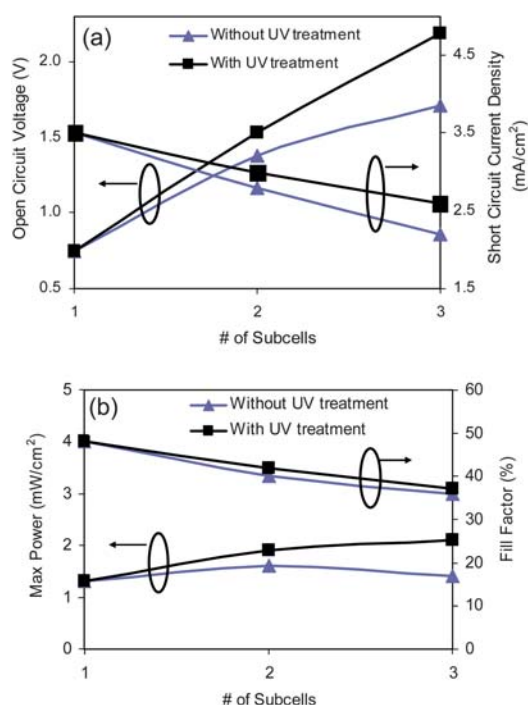


Fig. 15 Relation between the number of subcells and (a) the open circuit voltage (V_{oc}) and short circuit current density (J_{sc}); and (b) the maximum power output (P_{max}) and fill factor (FF) of a polymer multijunction solar cell using ZnO/modified PEDOT as interlayers with and without UV exposure treatment.¹⁹

bond breaks, releasing a volatile alkene and leaves the polymer component insoluble. A semitransparent intermediate layer comprising PEDOT:PSS and ZnO was spin coated as interlayers between the bottom and top subcells. Although the multijunction device showed poor performance (0.02%) due to inefficient single cells, high series resistance, and very low shunt resistance, it opened up a new way to fabricate PMSCs without concern for the choice of solvents for different individual subcells.

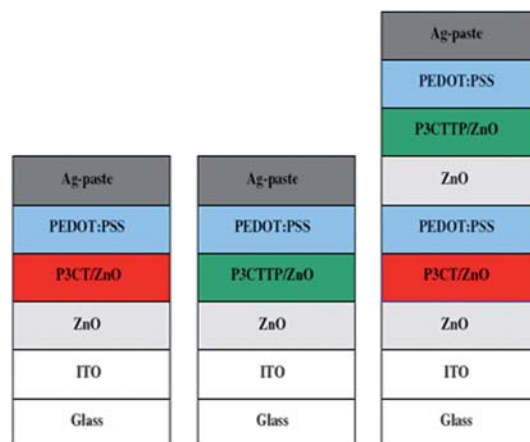


Fig. 16 Schematic representation of the single junction and multi-junction cells employing a wide band gap (P3CT) and a low band gap (P3CTTP) thermocleavable polymer materials. Reprinted with permission from ref. 53.

5.2.2 $\text{TiO}_{x(x \leq 2)}$ interlayer. So far, the most efficient all-solution processing double-junction organic solar cells have been reported by Kim *et al.*,⁹ with a 38% performance improvement compared to a single device. In this cell, a highly transparent titanium oxide ($\text{TiO}_{x(x \leq 2)}$) layer was used to separate the two subcells in the stack. Due to the highly transparent recombination layer, increased light intensity at the top subcell led to higher photocurrent generation. As a result, the efficiency of the double-junction device was not limited by the lower current of the top subcell as typically observed for multijunction structures with a semitransparent metallic interlayer. The cell was fabricated on a glass/ITO substrate covered by a 40 nm thick layer of PEDOT:PSS (Baytron P). The transparent $\text{TiO}_{x(x \leq 2)}$ interlayer was made by spin-coating from a methanol solution by sol-gel chemistry.⁵⁷ The bottom subcell was a 130 nm thick layer of PCPDTBT:PCBM film, made from a chlorobenzene based solution.⁹ The top subcell was a 170 nm thick P3HT:PC₇₀BM blend film, processed from a chloroform solution. It is noteworthy that the selective usage of PCBM or PC₇₀BM allowed reduction of spectral overlap in the two subcells and thereby ensured an optimized J_{sc} . The two subcells had complementary absorption spectra, which led to coverage of the entire visible and part of near infrared solar spectrum. The authors chose an “inverted multijunction cell” structure with a narrow bandgap PCPDTBT:PCBM composite as the bottom subcell and a wide bandgap P3HT:PC₇₀BM composite as the top subcell. They observed higher cell performance for this inverted layer sequence than that for the normal series structure. In order to make an efficient hole transport layer, a highly conductive PEDOT:PSS was spin-coated on top of the $\text{TiO}_{x(x \leq 2)}$ interlayer. The structure of this device is depicted in Fig. 17. An overall energy conversion efficiency of 6.5% was achieved using a solution processed $\text{TiO}_{x(x \leq 2)}$ interlayer.

5.3 Thermal evaporation

A highly transparent (98%), protective and structurally smooth film of Al (1 nm)/ MoO_3 (15 nm) was deposited by thermal evaporation as an intermediate layer in a triple-junction P3HT/PCBM polymer solar cell.⁵⁰ Fig. 18 shows the device configuration. Although identical P3HT/PCBM active layers were used to construct these triple-junction cells, an open circuit voltage of 1.73 V (0.62 V for single junction cells) and a power conversion efficiency of 2.03% were achieved under a simulated solar irradiation of 100 mW cm^{-2} (AM1.5G).

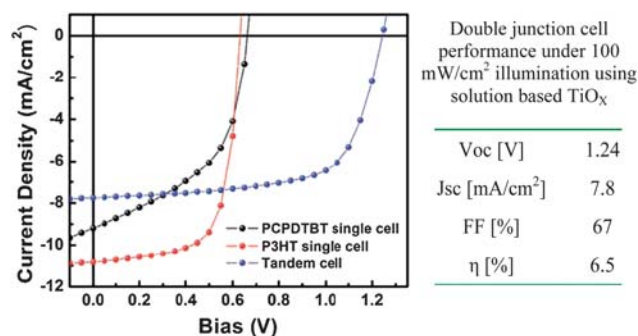


Fig. 17 Current density–voltage curves of the optical front subcell, back subcell, and double-junction cell. Reprinted with permission from ref. 9.

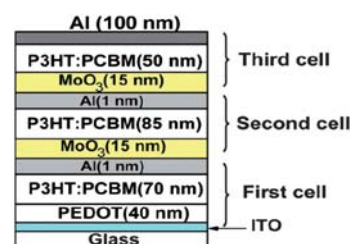


Fig. 18 Device configuration of a triple-junction polymer solar cell using thermally evaporated Al (1 nm)/ MoO_3 (15 nm) as interlayers. Reprinted with permission from ref. 50.

5.4 Combined solution processing and thermal evaporation

An interlayer consisting of an optical spacer layer and two carrier transport layers was reported by Hadipour *et al.*¹⁴ The interlayer was made by a combined thermal evaporation and solution processing method. The optical transmission window of the bottom subcell was optimized to match the optical absorption of the top subcell by varying the layer thickness of the optical spacer. The absorption spectra of two subcells are complementary with $\lambda_{max} \sim 850 \text{ nm}$ for the top and $\lambda_{max} \sim 550 \text{ nm}$ for the bottom subcell. The carrier transport layer for the bottom and top subcells was evaporated with Sm (3 nm)/Au (12 nm), and Au (20 nm), respectively. Then 250 nm of polytrifluoroethylene (PTFE), dissolved in methyl ethyl ketone (MEK), was spin coated onto the bottom subcell as an optical spacer layer. In this structure, the subcells could be electrically connected in series or parallel using four electrical contacts. The cell configuration is depicted in Fig. 19. The open circuit voltage (V_{oc}) in the series configuration was 1 V and equal to the sum of the V_{oc} s of both subcells. The short circuit current density (J_{sc}) in the parallel configuration was 9.2 mA cm^{-2} and equal to the sum of J_{sc} of both subcells. The cell performance in parallel configuration was higher than that in the series configuration.

6. Current challenges in PMSCs

Although significant progress has been made in polymer multijunction solar cells, energy conversion efficiencies are still too low for commercialization. In order to significantly increase

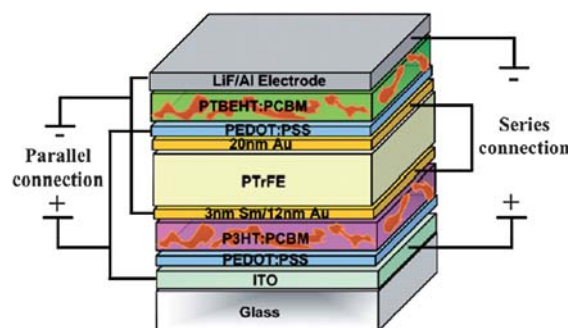


Fig. 19 Schematic diagram of a polymer multijunction solar cell using an optical spacer layer and two carrier transport layers as interlayers, which were deposited using a combined solution processing and thermal evaporation method. Reprinted with permission from ref. 14 and 27.

multijunction cell efficiency, the following challenges must be addressed:

- 1) Identification of efficient photovoltaic materials with broad spectrum light harvesting.
- 2) Identification of highly efficient interfacial layer materials as both protection and recombination layers.
- 3) Design of multilayer structures to ensure identical current generated by each subcell.

6.1 Identification of efficient photovoltaic materials with broad spectrum light harvesting

New conjugated polymers for donor materials should have low bandgaps to absorb broad spectrum sunlight, especially the low energy photons, which are currently not efficiently absorbed.^{38,67,68} Moreover, the absorption regions of different subcell layers need to have a considerable overlap to avoid a gap between the absorption spectra in two adjacent subcells.⁶⁹ A synthetic approach to tuning bandgaps of polymeric semiconductors is to include moieties from electron rich (donor), electron poor (acceptor), and donor–acceptor–donor (D–A–D) structures on the polymer backbone.^{9,36,70} Low bandgaps can be obtained by the D–A–D strategy because it takes advantage of the donor's high valence band (HOMO) and the acceptor's low conduction band (LUMO) to induce low bandgap compression in the hybrid molecule. In addition, some fullerenes and their derivatives, as acceptor materials, also help to improve light harvesting by complementing the absorption valley between the donor polymers.⁷¹ For example, PC₇₀BM was reported to efficiently absorb the light in the regions between two absorption peaks at 416 and 584 nm for PF-co-DTB based solar cells and led to higher power conversion efficiency than the widely-used PC₆₀BM.⁷¹

As shown in Fig. 20 for the photon flux solar spectrum, the majority of the photon flux is in the region 300 to 1500 nm, which accounts about 90% of the total cumulative photon flux. New materials with a combined light absorption regions that cover 300–1500 nm will be needed to significantly increase polymer multijunction solar cell efficiency.

If a combination of conjugated polymers with a bandgap of 2.0 eV (*e.g.* P3HT⁹), 1.4 eV (*e.g.* PCPDTBT⁹), and 0.8–0.9 eV (*e.g.* PBTTQ, PDDTT^{36,37,70}), respectively, are used to fabricate a triple junction polymer solar cell, they will each harvest about 1.2×10^{21} photons $\text{m}^{-2} \text{s}^{-1}$ in their corresponding subcells under an assumption of the same IPCE. As is shown in Fig. 21, they will absorb light in three spectral regions with equal photon flux: 390–600 nm, 600–900 nm, and 900–1500 nm, with each region accounting for about 30% of total photon flux. If one assumes an IPCE = 0.6, FF = 0.65, $\text{LUMO}_{\text{donor}} - \text{LUMO}_{\text{acceptor}} = 0.4$ eV for each subcell, then energy conversion efficiency as high as 15% can be achieved with $J_{\text{sc}} = 115 \text{ A m}^{-2}$ and $V_{\text{oc}} = 2 \text{ V}$.

6.2 Identification of highly efficient interfacial layer materials as both protection and recombination layer

If no interfacial contact is applied, an opposite junction will be formed between the acceptor layer in one subcell and donor layer in its adjacent subcell. Thus a middle contact layer has to be inserted between the adjacent subcells as a recombination center

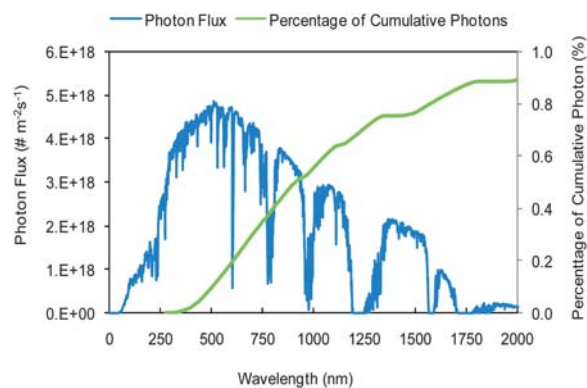


Fig. 20 The AM1.5 global photon flux spectrum and the percentage of the cumulative photon flux showing that the majority of the solar photons are located in the spectral region of 300–1500 nm.

for electrons and holes from their respective subcells. This layer will prevent the build-up of charges within the multijunction subcells, and help the Fermi levels in adjacent subcells to align to reduce the photovoltage loss.³⁰

A metal nanocluster (*e.g.*, Au, Ag) or a large bandgap metal oxide (*e.g.* TiO_x, ZnO) layer was used for this function.^{9,14–20,72–76} The interfacial middle contact has three different purposes: (1) a protective layer for the bottom subcell; (2) a foundation for the top subcell; and (3) an electrical contact between the two adjacent subcells *via* efficient electron–hole recombination. This layer could be inserted by dc magnetron sputtering (*e.g.* ITO),¹⁷ thermal evaporation (*e.g.* Sn, Au, Ag, WO₃),^{14,19} dip coating (*e.g.* TiO₂) and spin coating (*e.g.* ZnO).¹⁹ This interfacial layer is required to be transparent so that the lower energy photons can penetrate through, but does not need to have a high conductivity, since it does not necessarily transmit current.³⁰ The effectiveness of recombination layer is vital in multijunction solar cells because a poor recombination rate will lead to the build-up of local electric field and potential, thus reducing the overall cell efficiency.³⁰

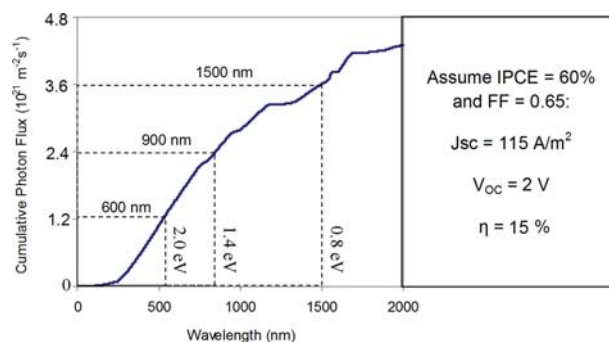


Fig. 21 Photon absorption in different regions with an equal photon flux: 350–600 nm, 600–900 nm, and 900–1500 nm, with each region accounting for 30% of total photon flux; and the estimation of the achievable energy conversion efficiency of a triple junction polymer solar cell. A device performance with an efficiency (η) of 15% is achievable from calculation.

Table 6 Non-exclusive list of the research progress in multifunction polymer solar cells as reported annually from 2006 to 2009

Year	Device Structure	Connection	J_{sc}/mAcm^{-2}	V_{oc}/V	FF (%)	PCE (%)	Ref.
2006	ITO/PEDOT:PSS/P3HT:PCBM/ ITO/ZnPc/ZnPc:C60/C60/Cr/AI	Normal series	4.8	1.02	45	2.3	18
	ITO/PEDOT:PSS/MEH- PPV:PCBM/LiF/AI/Au/MEH- PPV:PCBM/LiF/AI/Au	Mechanically stacked (series)	3.4	1.64	45	2.4 ± 0.2	22
		Mechanically stacked (parallel)	6.3	0.84	45	2.5 ± 0.1	
	ITO/Cr : Au:PEDOT/ PFDTBT:PCBM/LiF : AI/ Au:PEDOT/PTBEHT:PCBM/ LiF/AI	Normal series	~ 9	1.4	55	0.57	29
	ITO/PEDOT/P3HT:PCBM/ Sm : Au/PTTrFE/Au:PEDOT/ PTBEHT:PCBM/LiF : AI	Normal series	1.63	1.03	51	0.86 (calculated)	14
		Parallel	9.2	0.59	55	2.99 (estimated)	
2007	ITO/AI/LiF/APFOGreen9:PCBM/ APFO3:PCBM/PEDOT:PSS/ LiF/AI/ITO	Folded reflective	4.9	1.54	49	3.7	23
	ITO/PEDOT:PSS/MDMO- PPV:PCBM/ZnO/Modified PEDOT/P3HT:PCBM/LiF/AI	Normal series (double junction)	3.0	1.53	42	1.9	19
	ITO/PEDOT:PSS/MDMO- PPV:PCBM/ZnO/MDMO- PPV:PCBM/ZnO/Modified PEDOT/P3HT:PCBM/LiF/AI	Normal series (triple junction)	2.6	2.19	37	2.1	9
	ITO/PEDOT:PSS/ PCPDTBT:PCBM/TiO _x / PEDOT:PSS/P3HT:C ₇₀ PCBM/ TiO _x /AI	Inverted series	7.8	1.24	67	6.5	
			~ 0.54	0.54	24.6	0.07	53
2008	ITO/ZnO/P3CT:ZnO/ PEDOT:PSS/ZnO/ P3CTTP:ZnO/PEDOT:PSS/Ag	Inverted series					
	ITO/PEDOT:PSS/P3HT:PCBM/ LiF-MoO ₃ /CuPc/CuPc:C ₆₀ /C ₆₀ / Ag	Normal series	6.05	1.01	46.2	2.82	77
2009	ITO/PEDOT:PSS/P3HT:PCBM/ Al-MoO ₃ /P3HT:PCBM/Al- MoO ₃ /P3HT:PCBM/Al	Normal series (triple junction)	2.45	1.73	48.4	2.03	50
	ITO/PbSe NC QDs/PEDOT:PSS/ P3HT:PCBM/Al	Self-passivating	6.38	0.57	32.2	1.17	24

6.3 Design of multilayer structures to ensure identical current generated by each subcell

The overall current is determined by the lowest current produced by the individual subcells in the stack. The current of each subcell can be optimized to be equal to the others at the operating illumination intensity.^{14,30} Otherwise, the extra charges will build some local potential and electric field, and thus reduce device efficiency. The individual subcell currents are typically optimized by varying the thicknesses or material composition of the active materials in each subcell. If a combination of light-harvesting conjugated polymers is selected, film thickness can be used to balance the currents in individual cells in the stack. In addition, optical interference effects and thickness-dependent optical properties of the interfacial contact layers will also need be studied for structure optimization.³⁰ The highest short-circuit current (I_{sc}) in each subcell can be recorded, and then the lowest current can be increased to improve the overall current.

7. Conclusions

Polymer solar cells have attracted extensive scientific and commercial interest in the last decade due to their low cost, lightweight and mechanical flexibility. The multijunction

structure has become a potential approach to significantly increase energy conversion efficiency and the recent research progress is summarized in Table 6. Under reasonable assumptions, the achievable cell efficiencies for double-, triple- and quadruple- junction are 19%, 22%, and 24%, respectively. It is noteworthy that a highest achievable quadruple-junction cell efficiency (24%) is almost an improvement by a factor of two over that (10–13%) of a single junction solar cell under similar assumptions. In order to reach this theoretical efficiency, the spectral bandwidth of optical absorption of each active layer has to be improved. The entire visible and near infrared regions of sunlight need to be absorbed by employing two (or more) donor polymers with different absorption spectra in each active layer of a multijunction structure. In spite of vast variations in multijunction structures, the interfacial layers that separate subcells play a very important role. The interfacial layer serves as a recombination site only for the series configuration and therefore does not require high conductivity; however, in the parallel configuration, the sheet-conductivity has to be high since the contact is also used to extract the charges from the device.³⁰ The overall performance depends directly on the electrical (Ohmic contact and proper conductivity) and optical (transparency) properties of the interfacial layers. This review reveals that recently developed multijunction photovoltaic cells with

optimized materials, interfacial layers, as well as various device structures may lead to higher efficiencies as compared to single junction solar cells. Highly efficient polymer multijunction solar cells with power-conversion efficiencies of 6.5% have been reported by Heeger's group using an all-solution processed polymer multijunction structure.⁹ At present the trend of improving polymer multijunction photovoltaic cells as well as single junction cells indicates great potential for large-scale, cost effective, and clean energy production and commercialization.

References

- 1 B. Li, L. Wang, B. Kang, P. Wang and Y. Qiu, *Sol. Energy Mater. Sol. Cells*, 2006, **90**, 549–573.
- 2 P. V. Kamat, *J. Phys. Chem. C*, 2007, **111**, 2834–2860.
- 3 S.-S. Sun and N. S. Sariciftci, *Organic photovoltaics: mechanism, materials, and devices*, CRC Press, Boca Raton, 2005.
- 4 P. Taraneekar, Q. Qiao, J. Jiang, K. S. Schanze and J. R. Reynolds, *J. Am. Chem. Soc.*, 2007, **129**, 8958–8959.
- 5 Q. Qiao, Y. Xie and J. J. T. McLeskey, *J. Phys. Chem. C*, 2008, **112**, 9912–9916.
- 6 S. B. Darling, *Energy Environ. Sci.*, 2009, **2**, 1266–1273.
- 7 N. S. Sariciftci, L. Smilowitz, A. J. Heeger and F. Wudl, *Science*, 1992, **258**, 1474–1476.
- 8 H.-Y. Chen, J. Hou, S. Zhang, Y. Liang, G. Yang, Y. Yang, L. Yu, Y. Wu and G. Li, *Nat. Photonics*, 2009, **3**, 649–653.
- 9 J. Y. Kim, K. Lee, N. E. Coates, D. Moses, T. Q. Nguyen, M. Dante and A. J. Heeger, *Science*, 2007, **317**, 222–225.
- 10 G. Li, *SPIE: Org. Photovoltaics*, 2009, 7416–15.
- 11 <http://www.solarmer.com/news.php>, 2009.
- 12 S. E. Shaheen, D. S. Ginley and G. E. Jabbour, *MRS Bull.*, 2005, **30**, 10–19.
- 13 L. L. Kazmerski, *J. Electron Spectrosc. Relat. Phenom.*, 2006, **150**, 105–135.
- 14 A. Hadipour, B. de Boer and P. W. M. Blom, *J. Appl. Phys.*, 2007, **102**, 074506.
- 15 C.-W. Chen, Y.-J. Lu, C.-C. Wu, E. H.-E. Wu, C.-W. Chu and Y. Yang, *Appl. Phys. Lett.*, 2005, **87**, 241121.
- 16 A. G. F. Janssen, T. Riedl, S. Hamwi, H. H. Johannes and W. Kowalsky, *Appl. Phys. Lett.*, 2007, **91**, 073519.
- 17 K. Kawano, N. Ito, T. Nishimori and J. Sakai, *Appl. Phys. Lett.*, 2006, **88**, 073514.
- 18 G. Dennler, H.-J. Prall, R. Koeppel, M. Egginger, R. Autengruber and N. S. Sariciftci, *Appl. Phys. Lett.*, 2006, **89**, 073502.
- 19 J. Gilot, M. M. Wienk and R. A. J. Janssen, *Appl. Phys. Lett.*, 2007, **90**, 143512.
- 20 A. Yakimov and S. R. Forrest, *Appl. Phys. Lett.*, 2002, **80**, 1667–1669.
- 21 C. Zhang, S. W. Tong, C. Jiang, E. T. Kang, D. S. H. Chan and C. Zhu, *Appl. Phys. Lett.*, 2008, **92**, 083310.
- 22 V. Shrotriya, E. H.-E. Wu, G. Li, Y. Yao and Y. Yang, *Appl. Phys. Lett.*, 2006, **88**, 064104.
- 23 K. Tvingstedt, V. Andersson, F. Zhang and O. Inganas, *Appl. Phys. Lett.*, 2007, **91**, 123514.
- 24 S. J. Kim, W. J. Kim, A. N. Cartwright and P. N. Prasad, *Sol. Energy Mater. Sol. Cells*, 2009, **93**, 657–661.
- 25 M. C. Scharber, D. Mühlbacher, M. Koppe, P. Denk, C. Waldauf, A. J. Heeger and C. J. Brabec, *Adv. Mater.*, 2006, **18**, 789–794.
- 26 S. H. Park, A. Roy, S. Beaupre, S. Cho, N. Coates, J. S. Moon, D. Moses, M. Leclerc, K. Lee and A. J. Heeger, *Nat. Photonics*, 2009, **3**, 297–302.
- 27 T. Ameri, G. Dennler, C. Lungenschmied and C. J. Brabec, *Energy Environ. Sci.*, 2009, **2**, 347–363.
- 28 G. Dennler, M. C. Scharber, T. Ameri, P. Denk, K. Forberich, C. Waldauf and C. J. Brabec, *Adv. Mater.*, 2008, **20**, 579–583.
- 29 A. Hadipour, B. de Boer, J. Brabec, J. Wildeman, F. B. Kooistra, J. C. Hummelen, M. G. R. Turbiez, M. M. Wienk, R. A. J. Janssen and P. W. M. Blom, *Adv. Funct. Mater.*, 2006, **16**, 1897–1903.
- 30 P. Peumans, A. Yakimov and S. R. Forrest, *J. Appl. Phys.*, 2003, **93**, 3693–3723.
- 31 A. Hadipour, B. de Boer and P. W. M. Blom, *Org. Electron.*, 2008, **9**, 617–624.
- 32 W. L. Ma, C. Y. Yang, X. Gong, K. Lee and A. J. Heeger, *Adv. Funct. Mater.*, 2005, **15**, 1617–1622.
- 33 Y. Liang, Y. Wu, D. Feng, S.-T. Tsai, H.-J. Son, G. Li and L. Yu, *J. Am. Chem. Soc.*, 2009, **131**, 56–57.
- 34 G.-M. Ng, E. L. Kietzke, T. Kietzke, L.-W. Tan, P.-K. Liew and F. Zhu, *Appl. Phys. Lett.*, 2007, **90**, 103505.
- 35 M. Al-Ibrahim, S. Sensfuss, J. Uziel, G. Ecke and O. Ambacher, *Sol. Energy Mater. Sol. Cells*, 2005, **85**, 277–283.
- 36 A. P. Zoombelt, M. Fonrodona, M. M. Wienk, A. B. Sieval, J. C. Hummelen and R. A. J. Janssen, *Org. Lett.*, 2009, **11**, 903–906.
- 37 Y. Xia, L. Wang, X. Deng, D. Li, X. Zhu and Y. Cao, *Appl. Phys. Lett.*, 2006, **89**, 081106.
- 38 M. M. Wienk, M. G. R. Turbiez, M. P. Struijk, M. Fonrodona and R. A. J. Janssen, *Appl. Phys. Lett.*, 2006, **88**, 153511.
- 39 D. Mühlbacher, M. Scharber, M. Morana, Z. Zhu, D. Waller, R. Gaudiana and C. J. Brabec, *Adv. Mater.*, 2006, **18**, 2884–2889.
- 40 C. J. Brabec, C. Winder, N. S. Sariciftci, J. C. Hummelen, A. Dhanabalan, P. A. van Hal and R. A. J. Janssen, *Adv. Funct. Mater.*, 2002, **12**, 709–712.
- 41 G. Li, V. Shrotriya, J. Huang, Y. Yao, T. Moriarty, K. Emery and Y. Yang, *Nat. Mater.*, 2005, **4**, 864–868.
- 42 C. J. Brabec, S. E. Shaheen, C. Winder, N. S. Sariciftci and P. Denk, *Appl. Phys. Lett.*, 2002, **80**, 1288–1290.
- 43 M.-H. Chen, J. Hou, Z. Hong, G. Yang, S. Sista, L.-M. Chen and Y. Yang, *Adv. Mater.*, 2009, **21**, 4238–4242.
- 44 X. Wang, E. Perzon, J. L. Delgado, P. d. l. Cruz, F. Zhang, F. Langa, M. Andersson and O. Inganas, *Appl. Phys. Lett.*, 2004, **85**, 5081–5083.
- 45 E. Bundgaard and F. C. Krebs, *Sol. Energy Mater. Sol. Cells*, 2007, **91**, 954–985.
- 46 L. M. Campos, A. Tontcheva, S. Gunes, G. Sonmez, H. Neugebauer, N. S. Sariciftci and F. Wudl, *Chem. Mater.*, 2005, **17**, 4031–4033.
- 47 C. Winder, G. Matt, J. C. Hummelen, R. A. J. Janssen, N. S. Sariciftci and C. J. Brabec, *Thin Solid Films*, 2002, **403–404**, 373–379.
- 48 C. Shi, Y. Yao, Y. Yang and Q. Pei, *J. Am. Chem. Soc.*, 2006, **128**, 8980–8986.
- 49 Y. Kim, M. Shin, I. Lee, H. Kim and S. Heutz, *Appl. Phys. Lett.*, 2008, **92**, 093306.
- 50 D. W. Zhao, X. W. Sun, C. Y. Jiang, A. Kyaw, G. Q. Lo and D. L. Kwong, *IEEE Electron Device Lett.*, 2009, **30**, 490–492.
- 51 A. Chakrabarti, K. Hermann, R. Druzinic, M. Witko, F. Wagner and M. Petersen, *Phys. Rev. B: Condens. Matter Mater. Phys.*, 1999, **59**, 10583.
- 52 J. Ouyang, C. W. Chu, F. C. Chen, Q. Xu and Y. Yang, *Adv. Funct. Mater.*, 2005, **15**, 203–208.
- 53 O. Hagemann, M. Bjerring, N. C. Nielsen and F. C. Krebs, *Sol. Energy Mater. Sol. Cells*, 2008, **92**, 1327–1335.
- 54 Y. Ohsawa and T. Saji, *J. Chem. Soc., Chem. Commun.*, 1992, 781–782.
- 55 F. Louwet, L. Groenendaal, J. Dhaen, J. Manca, J. Van Luppen, E. Verdonck and L. Leenders, *Synth. Met.*, 2003, **135–136**, 115–117.
- 56 J. Gillot, I. Barbu, M. M. Wienk and R. A. J. Janssen, *Appl. Phys. Lett.*, 2007, **91**, 113520.
- 57 J. Y. Kim, S. H. Kim, H.-H. Lee, K. Lee, W. Ma, X. Gong and A. J. Heeger, *Adv. Mater.*, 2006, **18**, 572–576.
- 58 T. Trupke and P. Würfel, *J. Appl. Phys.*, 2004, **96**, 2347–2351.
- 59 M. Lenes, L. J. A. Koster, V. D. Mihailetschi and P. W. M. Blom, *Appl. Phys. Lett.*, 2006, **88**, 243502.
- 60 Y. Zhou, F. Zhang, K. Tvingstedt, W. Tian and O. Inganas, *Appl. Phys. Lett.*, 2008, **93**, 033302.
- 61 G. Li, V. Shrotriya, Y. Yao, J. Huang and Y. Yang, *J. Mater. Chem.*, 2007, **17**, 3126–3140.
- 62 C.-M. Yang, C.-H. Wu, H.-H. Liao, K.-Y. Lai, H.-P. Cheng, S.-F. Horng, H.-F. Meng and J.-T. Shy, *Appl. Phys. Lett.*, 2007, **90**, 133509.
- 63 W. J. E. Beek, M. M. Wienk and R. A. J. Janssen, *Adv. Mater.*, 2004, **16**, 1009–1013.
- 64 P. Claudia, K. Andreas and W. Horst, *Angew. Chem., Int. Ed.*, 2002, **41**, 1188–1191.
- 65 F. Verbakel, S. C. J. Meskers and R. A. J. Janssen, *Appl. Phys. Lett.*, 2006, **89**, 102103.
- 66 W. J. E. Beek, M. M. Wienk, M. Kemerink, X. Yang and R. A. J. Janssen, *J. Phys. Chem. B*, 2005, **109**, 9505–9516.
- 67 C.-P. Chen, S.-H. Chan, T.-C. Chao, C. Ting and B.-T. Ko, *J. Am. Chem. Soc.*, 2008, **130**, 12828–12833.

-
- 68 M. M. Wienk, M. Turbiez, J. Gilot and R. A. J. Janssen, *Adv. Mater.*, 2008, **20**, 2556–2560.
- 69 W. Mammo, S. Admassie, A. Gadisa, F. Zhang, O. Inganäs and M. R. Andersson, *Sol. Energy Mater. Sol. Cells*, 2007, **91**, 1010–1018.
- 70 X. Gong, M. Tong, Y. Xia, W. Cai, J. S. Moon, Y. Cao, G. Yu, C.-L. Shieh, B. Nilsson and A. J. Heeger, *Science*, 2009, **325**, 1665–1667.
- 71 Y. Yao, C. Shi, G. Li, V. Shrotriya, Q. Pei and Y. Yang, *Appl. Phys. Lett.*, 2006, **89**, 153507.
- 72 J. Xue, S. Uchida, B. P. Rand and S. R. Forrest, *Appl. Phys. Lett.*, 2004, **85**, 5757–5759.
- 73 P. Peumans and S. R. Forrest, *Appl. Phys. Lett.*, 2001, **79**, 126–128.
- 74 S. Uchida, J. Xue, B. P. Rand and S. R. Forrest, *Appl. Phys. Lett.*, 2004, **84**, 4218–4220.
- 75 J. Xue, S. Uchida, B. P. Rand and S. R. Forrest, *Appl. Phys. Lett.*, 2004, **84**, 3013–3015.
- 76 P. Peumans, S. Uchida and S. R. Forrest, *Nature*, 2003, **425**, 158–162.
- 77 D. W. Zhao, X. W. Sun, C. Y. Jiang, A. K. K. Kyaw, G. Q. Lo and D. L. Kwong, *Appl. Phys. Lett.*, 2008, **93**, 083305.